International Journal of Mechanical Sciences 51 (2009) 583–597

Contents lists available at ScienceDirect

International Journal of Mechanical Sciences

journal homepage: www.elsevier.com/locate/ijmecsci

Analysis of composite finite wedges under anti-plane shear

Chih-Hao Chen [a,*], Chein-Lee Wang [a], Chien-Chung Ke [b]

[a] Department of Resources Engineering, National Cheng Kung University, Tainan 701, Taiwan, ROC
[b] Geotechnical Engineering Research Center, Sinotech Engineering Consultants, Inc., Taipei 110, Taiwan, ROC

ARTICLE INFO

Article history:
Received 22 December 2008
Received in revised form
2 June 2009
Accepted 5 June 2009
Available online 12 June 2009

Keywords:
Composite
Finite wedge
Anti-plane shear
Stress intensity factor

ABSTRACT

Problems of composite finite wedges under anti-plane shear applied on a circular arc are analyzed in this study. The considered conditions of radial edges are free–free, free–fixed, and fixed–fixed. A procedure that uses the finite Mellin transform and the Laplace transform is developed to solve these problems. Explicit solutions for displacement and stress fields are derived. Stress intensity factors (SIFs) of composite circular shafts with an interfacial edge crack are extracted from the derived stress fields, and the distributions for various loading angles are presented and discussed. It was found that if the loading angles are the same, free–free and fixed–fixed edge problems can be degenerated into single material problems. Uniform stresses were found along the interface in free–free and fixed–fixed edge problems. Solutions of a general loading case deduced from the derived results compare well with those obtained from finite element (FE) analyses.

1. Introduction

Wedge problems have been investigated by many researchers. In-plane stress analysis of an isotropic wedge was first conducted by Tranter [1] using the Mellin transform of the Airy stress function in cylindrical coordinates. Thereafter, a number of associated in-plane problems were extended to bi-materials and anisotropic materials, with emphasis placed on the order of the stress singularity and the stress distribution near the wedge apex [2–9]. For these problems, out-of-plane normal stresses/strains are relative to in-plane stresses/strains, and out-of-plane (anti-plane) shear stresses/strains are zero, which is due to the plane stress/strain condition being used. Studies which treated out-of-plane shear stresses/strains with zero in-plane stresses/strains used the generalized plane strain condition [10]. The wedges were usually regarded as sectors with infinite/finite radii using cylindrical coordinates. For cases with infinite radii [11–16], the order of the stress singularity as well as the stress distributions for a range near the wedge apex was determined. The corresponding SIFs were calculated using the assumption that the problems were in infinite domains. Nonetheless, the obtained SIF from the analysis of an infinite domain should be calibrated by a suitable geometric function to make it fit for an application. The true full-field stress distributions can be affected by all the boundaries in addition to the locations near the wedge apex. Accordingly, wedges with finite radii have been considered [17–21].

Stress analysis of a finite domain is helpful for the comprehensive understanding of a problem. Although there are some numerical methods [22,23] that can be used to determine the full-field stress distributions for a wedge problem, analytical expressions for a finite wedge under anti-plane shear deformation can be obtained using the methods of the integral transform [18]. SIF can then be represented by an equation with geometric factors for convenience. All previous studies, except for particular cases in Shahani [20] and Lin and Ma [21], considered a group of problems with materials subjected to anti-plane shear loads in radial directions. The conditions of the circular arc of the wedge were fixed or traction free. As a result, the solutions are accessible after the integral transforms. However, wedges with finite radii may be subjected to loads on the circular boundaries, especially in cases of crack problems. To this end, the present study considers another group of finite wedge problems. The tractions are subjected to a circular arc, and traction free or fixed conditions are imposed on the radial edges of the wedge.

In the present work, a procedure that uses the finite Mellin transform in conjunction with the Laplace transform is proposed for solving the stated problems. Based on the proposed procedure with the prescribed point loads, fundamental solutions for this type of anti-plane shear problem of a composite finite wedge as well as the corresponding SIFs are obtained. Solutions for related general loading

* Corresponding author. Tel.: +886 6 2757575 62809; fax: +886 6 2380421.
E-mail addresses: chenhowardch@gmail.com (C.-H. Chen), clwang@mail.ncku.edu.tw (C.-L. Wang), karis.ke@gmail.com (C.-C. Ke).

0020-7403/$ - see front matter © 2009 Elsevier Ltd. All rights reserved.
doi:10.1016/j.ijmecsci.2009.06.002

Nomenclature

a	radius of the finite wedge
A_{I}, A_{II}, A_{III}	coefficients of solution in the Mellin domain
B_{I}, B_{II}, B_{III}	coefficients of solution in the Mellin domain
c	strip of regularity in the complex plane of the Mellin domain
D_{I}, D_{II}, D_{III}	determinants of two-by-two matrices (characteristic functions)
D'_{II}	differential of D_{II}
$f^{(j)}$	function for the finite Mellin transformation
$f_2^{*(j)}$	function after applying the finite Mellin transformation
F	concentrated anti-plane shear force
FE	finite element
$H_{\mathrm{III}}^{(\mathrm{I})}$, $H_{\mathrm{III}}^{(\mathrm{II})}$, $H_{\mathrm{III}}^{(\mathrm{III})}$	normalized mode III stress intensity factors
j	material number ($j = 1, 2$)
$K_{\mathrm{III}}^{(\mathrm{I})}$, $K_{\mathrm{III}}^{(\mathrm{II})}$, $K_{\mathrm{III}}^{(\mathrm{III})}$	mode III stress intensity factors
$L[]$	applying the Laplace transform
$L^{-1}[]$	applying the inverse Laplace transform
$M_2[]$	applying the finite Mellin transform of the second kind
$M_2^{-1}[]$	applying the inverse finite Mellin transform of the second kind
ODE	ordinary differential equation
p	parameter in the kernel of the finite Mellin transform
p_-, p_+	negative and positive roots of $D_\Lambda = 0$ (Λ = I, II, III)
p_1, Λ	smallest positive root of $D_\Lambda = 0$ (Λ = I, II, III)
$p_{n,\ \mathrm{II}}$	positive roots of $D_{\mathrm{II}} = 0$ ($n = 1, 2, 3, \ldots$)
P	anti-plane shear pressure
r	cylindrical coordinate axis
R	ratio of material constants (μ_1/μ_2)
Re[]	real part
s	parameter in the kernel of the Laplace transform
SIF(s)	stress intensity factor(s)
$T_{\mathrm{III}}^{(\mathrm{I})}$, $T_{\mathrm{III}}^{(\mathrm{III})}$	normalized uniform stresses
v	strip of regularity in the complex plane of the Laplace domain
$W^{(j)}$, $W_{\mathrm{I}}^{(j)}$, $W_{\mathrm{II}}^{(j)}$, $W_{\mathrm{III}}^{(j)}$	anti-plane displacements of jth material
$W_2^{*(j)}$, $W_{2,I}^{*(j)}$	anti-plane displacements of jth material after applying the Mellin transform of the second kind
$\bar{W}_2^{*(j)}$, $\bar{W}_{2,I}^{*(j)}$	anti-plane displacements of jth material after applying the Mellin transform of the second kind and the Laplace transform
$W_{\mathrm{arc},\Lambda}^{(j)}$	anti-plane displacement of jth material for the studied case with Problem Λ (Λ = I, II, III)
z	cylindrical polar coordinate axis
∇^2	Laplacian operator
α	apex angle of each material of the finite wedge
β	loading angle of 1st material of the finite wedge
γ	loading angle of 2nd material of the finite wedge
δ	Dirac-delta function
μ_1, μ_2, μ_j	shear moduli
θ	cylindrical polar coordinate axis
Λ	problem Λ (Λ = I, II, III)
φ_2, φ_1	upper and lower bounds of β loading range for the studied case
ξ_2, ξ_1	upper and lower bounds of γ loading range for the studied case
τ_{rz}, $\tau_{\theta z}$	shear stresses in the rz-direction and in the θz-direction
$\tau_{rz}^{(j)}$, $\tau_{\mathrm{rz,I}}^{(j)}$, $\tau_{\mathrm{rz,II}}^{(j)}$, $\tau_{\mathrm{rz,III}}^{(j)}$	shear stresses in the rz-direction of jth material
$\tau_{\theta z}^{(j)}$, $\tau_{\theta \mathrm{z,I}}^{(j)}$, $\tau_{\theta \mathrm{z,II}}^{(j)}$, $\tau_{\theta \mathrm{z,III}}^{(j)}$	shear stresses in the θz-direction of jth material
$\tau_{\mathrm{arc}\ rz,\Lambda}^{(j)}$	shear stress in the rz-direction of jth material for the studied case with Problem Λ (Λ = I, II, III)
$\tau_{\mathrm{arc}\ \theta z,\Lambda}^{(j)}$	shear stress in the θz-direction of jth material for the studied case with Problem Λ (Λ = I, II, III)
$\Omega_\Lambda^{(j)}$	normalized displacement of jth material for the studied case with Problem Λ (Λ = I, II, III)
$\Gamma_\Lambda^{(j)}$	normalized shear stress in the rz-direction of jth material for the studied case with Problem Λ (Λ = I, II, III)
$\Theta_\Lambda^{(j)}$	normalized shear stress in the θz-direction of jth material for the studied case with Problem Λ (Λ = I, II, III)

problems can be obtained by integrating the derived fundamental solutions over the range of interest, as shown in Section 3. The results are compared with those obtained from FE analyses.

2. Problem formulation and solutions

Fig. 1 shows the composite wedge, with a finite radius a, considered in this study. The apex angle of each material is α, and the shear moduli are μ_1 and μ_2, respectively. An infinite length along the z-axis perpendicular to the plane is assumed. Accordingly, the problem belongs to the plane deformation type. The only displacement component in the z-direction is a function relative to the in-plane coordinates (r, θ). In this study, the circular arc of the wedge ($r = a$) is subjected to a pair of anti-plane concentrated forces, F, at angles $\theta = \beta$ and $\theta = -\gamma$. The shear stresses on the z-axis, τ_{rz} and $\tau_{\theta z}$, are the remaining components in the constitutive equations, which can be expressed as

$$\tau_{rz}^{(j)}(r,\theta) = \mu_j \frac{\partial W^{(j)}(r,\theta)}{\partial r} \tag{1}$$

$$\tau_{\theta z}^{(j)}(r,\theta) = \frac{\mu_j}{r} \frac{\partial W^{(j)}(r,\theta)}{\partial \theta} \tag{2}$$

where W is the displacement in the z-axis, and $j = 1, 2$ for the jth material.

The static equilibrium equation in the absence of body forces is

$$\frac{\partial [r\tau_{rz}^{(j)}(r,\theta)]}{\partial r} + \frac{\partial \tau_{\theta z}^{(j)}(r,\theta)}{\partial \theta} = 0 \tag{3}$$

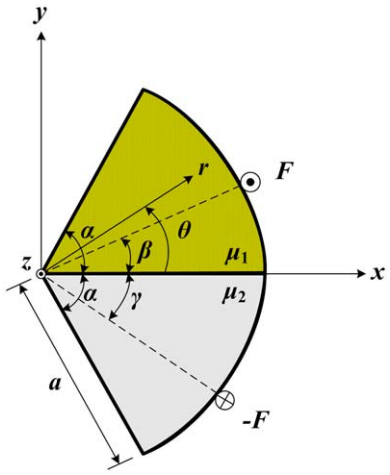

Fig. 1. Schematic view of the considered composite wedge subjected to a pair of concentrated anti-plane shear loads on a circular arc.

By substituting Eqs. (1) and (2) into Eq. (3), the equilibrium equation can be reduced to

$$\nabla^2 W^{(j)}(r,\theta) = 0 \tag{4}$$

where

$$\nabla^2 = \frac{\partial^2}{\partial r^2} + \frac{1}{r}\frac{\partial}{\partial r} + \frac{1}{r^2}\frac{\partial^2}{\partial \theta^2}$$

denotes the Laplacian operator.

The Mellin transform can be employed for solving Eq. (4). To deal with the traction boundary on the circular arc, the finite Mellin transform of the second kind is adopted [24]:

$$M_2[f^{(j)}(r,\theta);p] = f_2^{*(j)}(p,\theta) = \int_0^a (a^{2p}r^{-p-1} + r^{p-1}) f^{(j)}(r,\theta)\,dr \tag{5}$$

where p is a complex transform parameter. The inversion formula is in the form:

$$M_2^{-1}[f_2^{*(j)}(p,\theta);r] = f^{(j)}(r,\theta) = \frac{1}{2\pi i}\int_{c-i\infty}^{c+i\infty} r^{-p} f^{(j)}(p,\theta)\,dp \tag{6}$$

where $i = \sqrt{-1}$ and the constant $\mathrm{Re}[p] = c$ defines the path of integration in the complex plane.

Applying Eq. (5) to Eq. (4) yields

$$\left(\frac{d^2}{d\theta^2} + p^2\right) W_2^{*(j)}(p,\theta) + 2a^{p+1}\frac{\partial W^{(j)}(a,\theta)}{\partial r} = 0 \tag{7}$$

provided

$$\lim_{r\to 0}\left[(a^{2p}r^{-p+1} + r^{p+1})\frac{\partial W^{(j)}(r,\theta)}{\partial r} + p(a^{2p}r^{-p} - r^p) W^{(j)}(r,\theta)\right] = 0 \tag{8}$$

Eq. (8) can be used to define the path of the line integral $\mathrm{Re}[p] = c$ in Eq. (6); i.e., the strip of regularity should be determined from Eq. (8) such that the integral in Eq. (5) exists.

The prescribed boundary conditions are:

$$\tau_{rz}^{(j)}(a,\theta) = F[(2-j)\delta(\theta-\beta) + (1-j)\delta(\theta+\gamma)] \tag{9a}$$

$$W^{(j)}(0,\theta) = 0 \tag{9b}$$

where $\beta \le \alpha$, $\gamma \le \alpha$, $\alpha \le \pi$, and δ denotes the Dirac-delta function.

Applying Eq. (9) to Eq. (7) with the aid of Eq. (1) gives

$$\left(\frac{d^2}{d\theta^2} + p^2\right) W_2^{*(j)}(p,\theta) + \frac{2Fa^{p+1}}{\mu_j}[(2-j)\delta(\theta-\beta) + (1-j)\delta(\theta+\gamma)] = 0 \tag{10}$$

Eq. (10) is an ODE with a non-homogeneous term. Mathematically, this equation has a solution which is related to a trigonometric function that repeats periodically. Thus, this study regards the boundary-value problem of this kind as an initial-value problem.

The Laplace transform is [24]

$$L[W_2^{*(j)}(p,\theta);s] = \bar{W}_2^{*(j)}(p,s) = \int_0^{\infty} e^{-s\theta} W_2^{*(j)}(p,\theta)d\theta \tag{11}$$

where s is the transform parameter. The inverse of the Laplace transform in terms of Eq. (11) is given by

$$L^{-1}[\bar{W}_2^{*(j)}(p,s);\theta] = W_2^{*(j)}(p,\theta) = \frac{1}{2\pi i}\int_{\nu-i\infty}^{\nu+i\infty} e^{s\theta}\bar{W}_2^{*(j)}(p,s)ds \tag{12}$$

where the constant $\mathrm{Re}[s]=\nu$ defines the path of integration in the complex plane.

Taking the Laplace transform on both sides of Eq. (10) gives

$$(s^2+p^2)\bar{W}_2^{*(j)}(p,s) - sW_2^{*(j)}(p,0) + (-1)^j\frac{\partial W_2^{*(j)}(p,0)}{\partial\theta} = \frac{2Fa^{p+1}}{\mu_j}[(j-2)e^{-s\beta}+(j-1)e^{-s\gamma}] \tag{13}$$

where $W_2^{*(j)}(p,0)$ and $\partial W_2^{*(j)}(p,0)/\partial\theta$ are the initial boundary conditions in the Laplace domain to be determined, or the undetermined coefficients in the Mellin domain; they can be deduced from the boundary conditions prescribed on the radial edges (i.e., boundary conditions at $\theta=\pm\alpha$). Detailed solutions are presented below.

2.1. Problem I: Free–free edge

Traction-free radial edges are considered in Problem I. The corresponding boundary conditions are:

$$\tau_{\theta z,\mathrm{I}}^{(1)}(r,\alpha) = \tau_{\theta z,\mathrm{I}}^{(2)}(r,-\alpha) = 0 \tag{14a}$$

$$W_{\mathrm{I}}^{(1)}(r,0) = W_{\mathrm{I}}^{(2)}(r,0) \tag{14b}$$

$$\tau_{\theta z,\mathrm{I}}^{(1)}(r,0) = \tau_{\theta z,\mathrm{I}}^{(2)}(r,0) \tag{14c}$$

where the subscript I denotes Problem I in this study. After applying the finite Mellin transform (Eq. (5)) to Eq. (14), the radial boundary conditions are:

$$M_2[\tau_{\theta z,\mathrm{I}}^{(1)}(r,\alpha)] = M_2[\tau_{\theta z,\mathrm{I}}^{(2)}(r,-\alpha)] = 0 \tag{15a}$$

$$M_2[W_{\mathrm{I}}^{(1)}(r,0)] = M_2[W_{\mathrm{I}}^{(2)}(r,0)] \tag{15b}$$

$$M_2[r\tau_{\theta z,\mathrm{I}}^{(1)}(r,0)] = M_2[r\tau_{\theta z,\mathrm{I}}^{(2)}(r,0)] \tag{15c}$$

To solve Eq. (13), the following coefficients are assumed based on Eqs. (15b) and (15c):

$$M_2[W_{\mathrm{I}}^{(1)}(r,0)] = M_2[W_{\mathrm{I}}^{(2)}(r,0)] = A_I \tag{16}$$

$$M_2[r\tau_{\theta z,\mathrm{I}}^{(1)}(r,0)] = M_2[r\tau_{\theta z,\mathrm{I}}^{(2)}(r,0)] = B_I \tag{17}$$

After applying Eq. (17) with the aid of Eq. (2), the following relationship is obtained:

$$\frac{\partial W_{2,\mathrm{I}}^{*(j)}(p,0)}{\partial\theta} = \frac{B_{\mathrm{I}}}{\mu_j} \tag{18}$$

Substituting Eqs. (16) and (18) into Eq. (13) gives

$$\bar{W}_{2,\mathrm{I}}^{*(j)}(p,s) = \left(\frac{s}{s^2+p^2}\right)A_{\mathrm{I}} + (-1)^{j+1}\frac{1}{\mu_j}\left(\frac{1}{s^2+p^2}\right)B_{\mathrm{I}} + \left(\frac{1}{s^2+p^2}\right)\frac{2Fa^{p+1}}{\mu_j}[(j-2)e^{-s\beta}+(j-1)e^{-s\gamma}] \tag{19}$$

Applying the inverse Laplace transform (Eq. (12)) to Eq. (19) yields

$$W_{2,I}^{*(j)}(p,\theta) = A_I\cos(p\theta) + B_I\frac{\sin(p\theta)}{\mu_j p} - \frac{2Fa^{p+1}}{\mu_j p}\left\{\begin{array}{l}(2-j)H(\theta-\beta)\sin[p(\theta-\beta)]\\ +(1-j)H(\theta+\gamma)\sin[p(\theta+\gamma)]\end{array}\right\} \tag{20}$$

where H is the Heaviside function. After applying Eq. (15a) with the aid of Eq. (2), the coefficients A_{I} and B_{I} can be solved:

$$A_{\mathrm{I}} = \frac{Fa^{p+1}\cos(p\alpha)\{\cos[p(\alpha-\gamma)]-\cos[p(\alpha-\beta)]\}}{D_{\mathrm{I}}(p)} \tag{21}$$

$$B_{\mathrm{I}} = \frac{Fa^{p+1}p\,\sin(p\alpha)\{\mu_1\,\cos[p(\alpha-\gamma)]+\mu_2\,\cos[p(\alpha-\beta)]\}}{D_{\mathrm{I}}(p)} \tag{22}$$

where

$$D_{\mathrm{I}}(p) = p(\mu_1+\mu_2)\sin(2p\alpha) \tag{23}$$

The zeros of $D_{\mathrm{I}}(p)$ determine the order of the stress singularity at the wedge apex. The orders of the stress singularity for bi-material wedge problems under anti-plane shear deformation were discussed in previous studies [12,16]. The behavior of the stress singularity

depends on the conditions of the radial edges. The characteristic functions, Eq. (23), as well as those in the following sections, obtained in this study are identical to those in previous studies since the same conditions of radial edges are used.

By applying the inverse finite Mellin transform (Eq. (6)) in conjunction with the residue theorem, the displacement field is derived as

$$W_{\mathrm{I}}^{(j)}(r,\theta)=\frac{2Fa}{(\mu_1+\mu_2)\pi}\times\sum_{n=1}^{\infty}\begin{Bmatrix}\dfrac{2}{2n-1}\left\{R^{j-1}\sin\left[\dfrac{(2n-1)\pi}{2\alpha}\gamma\right]+R^{j-2}\sin\left[\dfrac{(2n-1)\pi}{2\alpha}\beta\right]\right\}\sin\left[\dfrac{(2n-1)\pi}{2\alpha}\theta\right]\left(\dfrac{r}{a}\right)^{(2n-1)\pi/2\alpha}\\ -\dfrac{1}{n}\left[\cos\left(\dfrac{n\pi\gamma}{\alpha}\right)-\cos\left(\dfrac{n\pi\beta}{\alpha}\right)\right]\cos\left(\dfrac{n\pi\theta}{a}\right)\left(\dfrac{r}{a}\right)^{n\pi/\alpha}\end{Bmatrix} \tag{24}$$

where

$$R=\frac{\mu_1}{\mu_2} \tag{25}$$

It should be noted that the path of integration for inversion integrals is within the strip of regularity $\mathrm{Re}[p]<0$, but we replace p_- (negative p) by $-\mathrm{p}_+$ (positive p) here.

The corresponding stress fields are:

$$\tau_{rz,\mathrm{I}}^{(j)}(r,\theta)=\frac{2F}{(R+1)\alpha}\times\sum_{n=1}^{\infty}\begin{Bmatrix}\left\{R\sin\left[\dfrac{(2n-1)\pi}{2\alpha}\gamma\right]+\sin\left[\dfrac{(2n-1)\pi}{2\alpha}\beta\right]\right\}\sin\left[\dfrac{(2n-1)\pi}{2\alpha}\theta\right]\left(\dfrac{r}{a}\right)^{((2n-1)\pi/2\alpha)-1}\\ -R^{2-j}\left[\cos\left(\dfrac{n\pi\gamma}{\alpha}\right)-\cos\left(\dfrac{n\pi\beta}{\alpha}\right)\right]\cos\left(\dfrac{n\pi\theta}{\alpha}\right)\left(\dfrac{r}{a}\right)^{(n\pi/\alpha)-1}\end{Bmatrix} \tag{26}$$

$$\tau_{\theta z,I}^{(j)}(r,\theta)=\frac{2F}{(R+1)\alpha}\times\sum_{n=1}^{\infty}\begin{Bmatrix}\left\{R\sin\left[\dfrac{(2n-1)\pi}{2\alpha}\gamma\right]+\sin\left[\dfrac{(2n-1)\pi}{2\alpha}\beta\right]\right\}\cos\left[\dfrac{(2n-1)\pi}{2\alpha}\theta\right]\left(\dfrac{r}{a}\right)^{((2n-1)\pi/2\alpha)-1}\\ +R^{2-j}\left[\cos\left(\dfrac{n\pi\gamma}{\alpha}\right)-\cos\left(\dfrac{n\pi\beta}{\alpha}\right)\right]\sin\left(\dfrac{n\pi\theta}{\alpha}\right)\left(\dfrac{r}{a}\right)^{(n\pi/\alpha)-1}\end{Bmatrix} \tag{27}$$

For $R=1$ and $\beta=\gamma$, the solution is identical to that for the anti-symmetrical problem of the single material case in Shahani [20], which was obtained by the separation of variables.

When $\alpha=\pi$, a uniform $\tau_{rz,\mathrm{I}}^{(j)}$ is found at $\theta=0$:

$$\lim_{r\to 0}\tau_{rz,\mathrm{I}}^{(j)}(r,0)=\frac{2FR^{2-j}}{(R+1)\pi}[\cos(\beta)-\cos(\gamma)] \tag{28}$$

This shows that the uniform $\tau_{rz,\mathrm{I}}^{(j)}$ results from the discrepancy of the two loading angles. The following normalized expression is used for this uniform stress:

$$T_{\mathrm{III}}^{(\mathrm{I})}=\frac{(R+1)\pi}{2FR^{2-j}}\lim_{r\to 0}\tau_{rz,\mathrm{III}}^{(j)}(r,0) \tag{29}$$

where the superscript I denotes Problem I here. The $T_{\mathrm{III}}^{(\mathrm{I})}$ distribution for γ versus β is plotted in Fig. 2. If $\beta=\gamma$ and $\theta=0$, $T_{\mathrm{III}}^{(\mathrm{I})}$ is reduced to zero, and so are $\tau_{rz,\mathrm{I}}^{(j)}$ and $W_I^{(j)}$. This implies that if $\beta=\gamma$, the composite material problem can be regarded as two single material problems for which the interface is fixed.

The following SIF definition is used for an interfacial crack problem in this study:

$$K_{\mathrm{III}}^{(\Lambda)}=\lim_{r\to 0}\sqrt{2\pi}r^{1-p_{1,\Lambda}}\tau_{\theta z,\mathrm{I}}^{(j)}(r,0) \tag{30}$$

where $\Lambda=$ I, II and III for Problems I, II, and III, respectively. $P_{1,\Lambda}$ is the smallest positive root for $D_\Lambda(p)=0$.

The SIF of Problem I ($\alpha=\pi$) is

$$K_{\mathrm{III}}^{(\mathrm{I})}=\frac{2F}{(R+1)}\sqrt{\frac{2a}{\pi}}\left\{R\sin\left[\frac{\gamma}{2}\right]+\sin\left[\frac{\beta}{2}\right]\right\} \tag{31}$$

The normalized SIF for Problem I can be defined by

$$H_{\mathrm{III}}^{(\mathrm{I})}=\frac{K_{\mathrm{III}}^{(\mathrm{I})}(R+1)}{2F}\sqrt{\frac{\pi}{2a}} \tag{32}$$

The $H_{\mathrm{III}}^{(\mathrm{I})}$ distributions for γ versus β with $R=0.1$, 1, and 10 are plotted in Fig. 3. It can be seen that β dominates the magnitude of $H_{\mathrm{III}}^{(\mathrm{I})}$ for $R=0.1$ and that γ dominates the magnitude of $H_{\mathrm{III}}^{(\mathrm{I})}$ for $R=10$. This indicates that the loading angle of a stiffer material has a lesser effect on SIF. In addition, β and γ contribute equally to $H_{\mathrm{III}}^{(\mathrm{I})}$ for $R=1$, as expected.

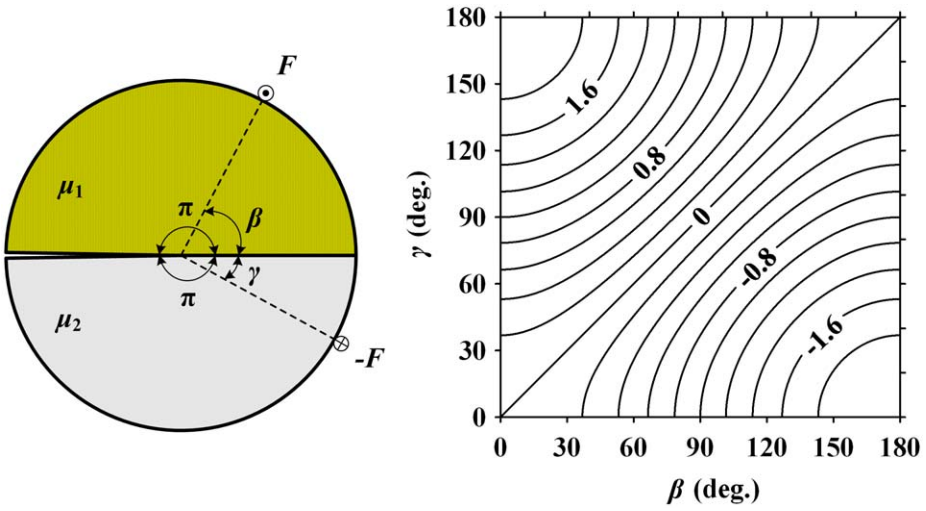

Fig. 2. $T_{\mathrm{II}}^{(\mathrm{I})}$ distribution for γ versus β in Problem I.

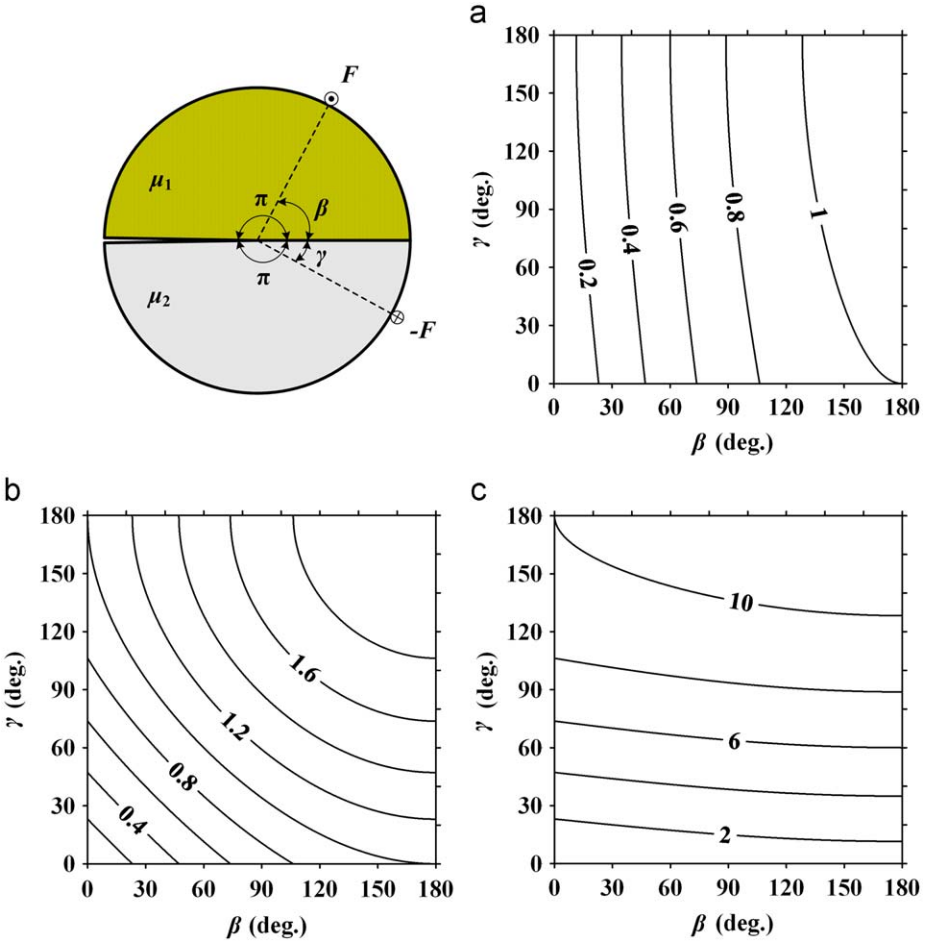

Fig. 3. $H_{\mathrm{II}}^{(\mathrm{I})}$ distributions for γ versus β in Problem I. (a) $R=0.1$, (b) $R=1$, (c) $R=10$.

2.2. Problem II: Free–fixed edge

The considered boundary conditions in the Mellin domain for Problem II are:

$$M_2[\tau_{\theta z,\mathrm{II}}^{(1)}(r,\alpha)] = M_2[W_{\mathrm{II}}^{(2)}(r,-\alpha)] = 0 \tag{33a}$$

$$M_2[W_{\mathrm{II}}^{(1)}(r,0)] = M_2[W_{\mathrm{II}}^{(2)}(r,0)] = A_{\mathrm{II}} \tag{33b}$$

$$M_2[r\tau^{(1)}_{\theta z,\mathrm{II}}(r,0)] = M_2[r\tau^{(2)}_{\theta z,\mathrm{II}}(r,0)] = B_{\mathrm{II}} \tag{33c}$$

where the subscript II denotes Problem II in this study. Similar to Problem I, the coefficients in the Mellin domain for Problem II are determined:

$$A_{\mathrm{II}} = \frac{2Fa^{p+1}\{\cos(p\alpha)\sin[p(\alpha-\gamma)] - \sin(p\alpha)\cos[p(\alpha-\beta)]\}}{D_{\mathrm{II}}(p)} \tag{34}$$

$$B_{\mathrm{II}} = \frac{2Fa^{p+1}p\{\mu_1\ \sin(p\alpha)\sin[p(\alpha-\gamma)] - \mu_2\ \cos(p\alpha)\cos[p(\alpha-\beta)]\}}{D_{\mathrm{II}}(p)} \tag{35}$$

where

$$D_{\mathrm{II}}(p) = p[\mu_1 \sin^2(p\alpha) - \mu_2\cos^2(p\alpha)] \tag{36}$$

The displacement field is derived as

$$W^{(j)}_{\mathrm{II}}(r,\theta) = \sum_{n=1}^{\infty}\left[\frac{2Fa}{D'_{\mathrm{II}}(p)}\left\{\begin{array}{l}\left\{\begin{array}{l}\sin(p\alpha)\cos[p(\alpha-\beta)]\\ -\cos(p\alpha)\sin[p(\alpha-\gamma)]\end{array}\right\}\cos(p\theta)\\ -\left\{\begin{array}{l}R^{j-1}\sin(p\alpha)\sin[p(\alpha-\gamma)]\\ -R^{j-2}cos(p\alpha)\cos[p(\alpha-\beta)]\end{array}\right\}\sin(p\theta)\end{array}\right\}\left(\frac{r}{a}\right)^{p}\right]_{p=p_{n,\mathrm{II}}} \tag{37}$$

where

$$D'_{\mathrm{II}}(p) = p\alpha(\mu_1+\mu_2)\sin(2p\alpha) \tag{38}$$

$$p_{n,\mathrm{II}} = \frac{1}{\alpha}\left[\tan^{-1}\left(\sqrt{\frac{1}{R}}\right) + (n-1)\pi\right] \quad \text{for } n = 1,3,5,\ldots \tag{39a}$$

$$p_{n,\mathrm{II}} = \frac{1}{\alpha}\left[n\pi - \tan^{-1}\left(\sqrt{\frac{1}{R}}\right)\right] \quad \text{for } n = 2,4,6,\ldots \tag{39b}$$

Note that $D'_{\mathrm{II}}(p_{n,\mathrm{II}})\neq 0$ can be obtained if $D'_{\mathrm{II}}(p_{n,\mathrm{II}}) = 0$. The corresponding stress fields are:

$$\tau^{(j)}_{rz,\mathrm{II}}(r,\theta) = \sum_{n=1}^{\infty}\left[\frac{2Fp\mu_j}{D'_{\mathrm{II}}(p)}\left\{\begin{array}{l}\left\{\begin{array}{l}\sin(p\alpha)\cos[p(\alpha-\beta)]\\ -\cos(p\alpha)\sin[p(\alpha-\gamma)]\end{array}\right\}\cos(p\theta)\\ -\left\{\begin{array}{l}R^{j-1}\sin(p\alpha)\sin[p(\alpha-\gamma)]\\ -R^{j-2}\cos(p\alpha)\cos[p(\alpha-\beta)]\end{array}\right\}\sin(p\theta)\end{array}\right\}\left(\frac{r}{a}\right)^{p-1}\right]_{p=p_{n,\mathrm{II}}} \tag{40}$$

$$\tau^{(j)}_{\theta z,\mathrm{II}}(r,\theta) = \sum_{n=1}^{\infty}\left[\frac{-2Fp\mu_j}{D'_{\mathrm{II}}(p)}\left\{\begin{array}{l}\left\{\begin{array}{l}\sin(p\alpha)\cos[p(\alpha-\beta)]\\ -\cos(p\alpha)\sin[p(\alpha-\gamma)]\end{array}\right\}\sin(p\theta)\\ +\left\{\begin{array}{l}R^{j-1}\sin(p\alpha)\sin[p(\alpha-\gamma)]\\ -R^{j-2}\cos(p\alpha)\cos[p(\alpha-\beta)]\end{array}\right\}\cos(p\theta)\end{array}\right\}\left(\frac{r}{a}\right)^{p-1}\right]_{p=p_{n,\mathrm{II}}} \tag{41}$$

The smallest admissible order of stress for Problem II is $1/\alpha\tan^{-1}(\sqrt{1/R}) - 1$. For $R = 1$ and $\alpha = 1/2\pi$ (the case of a single material with a crack), the square-root singularity is recovered.

Using the definition in Eq. (30), the SIF of Problem II ($\alpha = \pi$) is

$$K^{(\mathrm{II})}_{\mathrm{III}} = \frac{Fa^{1-p_{1,\mathrm{II}}}}{(R+1)}\sqrt{\frac{2}{\pi}}\{\sqrt{R}[\cos(p_{1,\mathrm{II}}\beta) - \cos(p_{1,\mathrm{II}}\gamma)] + \sin(p_{1,\mathrm{II}}\beta) + R\ \sin(p_{1,\mathrm{II}}\gamma)\} \tag{42}$$

where $p_{1,\mathrm{II}} = 1/\pi\tan^{-1}(\sqrt{1/R})$. The normalized SIF for Problem II can be defined by

$$H^{(\mathrm{II})}_{\mathrm{III}} = \frac{K^{(\mathrm{II})}_{\mathrm{III}}(R+1)}{Fa^{1-p_{1,\mathrm{II}}}}\sqrt{\frac{\pi}{2}} \tag{43}$$

The $H^{(\mathrm{II})}_{\mathrm{III}}$ distributions for γ versus β with $R = 0.1$, 1, and 10 are plotted in Fig. 4. The figure shows that increasing β has little effect on $H^{(\mathrm{II})}_{\mathrm{III}}$ for constant γ when $R = 10$. If $\mu_1 \gg \mu_2$, $H^{(\mathrm{II})}_{\mathrm{III}}$ is reduced to a function with respect to γ.

2.3. Problem III: Fixed–fixed edge

The considered boundary conditions for Problem III are:

$$M_2[W^{(1)}_{\mathrm{III}}(r,\alpha)] = M_2[W^{(2)}_{III}(r,-\alpha)] = 0 \tag{44a}$$

$$M_2[W^{(1)}_{\mathrm{III}}(r,0)] = M_2[W^{(2)}_{\mathrm{III}}(r,0)] = A_{\mathrm{III}} \tag{44b}$$

$$M_2[r\tau^{(1)}_{\theta z,\mathrm{III}}(r,0)] = M_2[r\tau^{(2)}_{\theta z,\mathrm{III}}(r,0)] = B_{\mathrm{III}} \tag{44c}$$

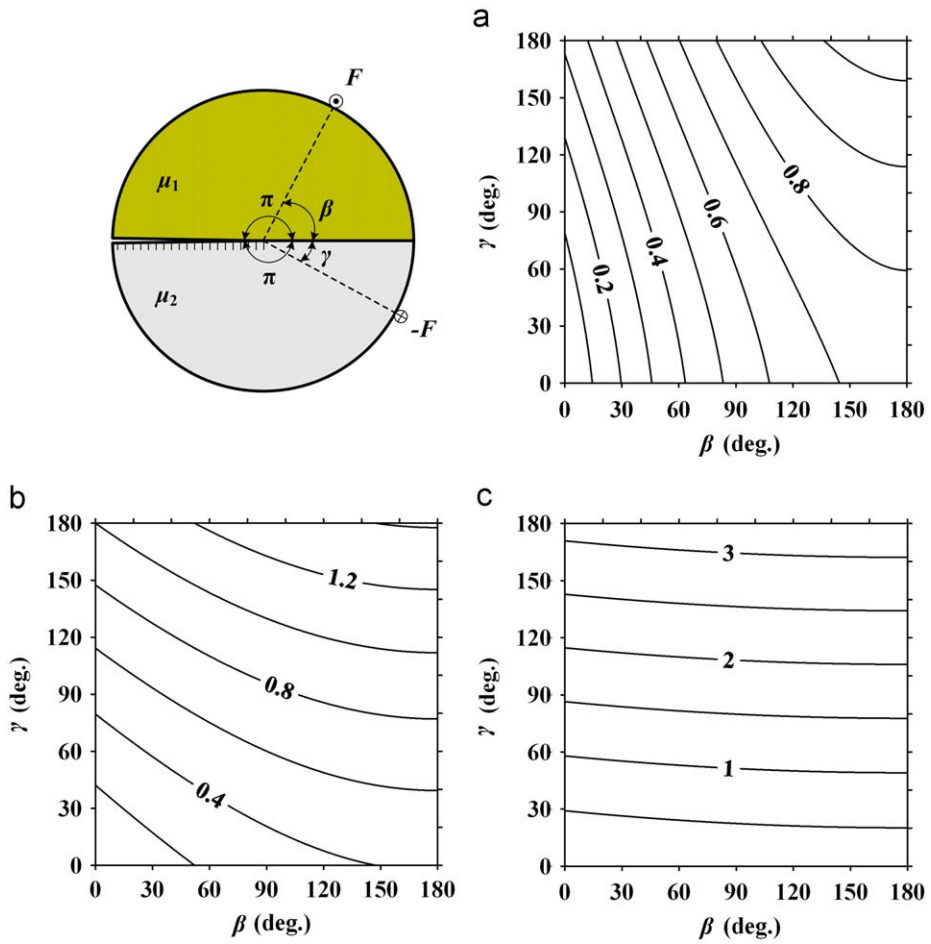

Fig. 4. $T_{III}^{(II)}$ distributions for γ versus β in Problem II. (a) $R = 0.1$, (b) $R = 1$, (c) $R = 10$.

where the subscript III denotes Problem III in this study. Similar to Problem I, the coefficients in the Mellin domain for Problem III are determined:

$$A_{III} = \frac{Fa^{p+1}\sin(p\alpha)\{\sin[p(\alpha-\beta)] - \sin[p(\alpha-\gamma)]\}}{D_{III}(p)} \tag{45}$$

$$B_{III} = \frac{Fa^{p+1}p\cos(p\alpha)\{\mu_1\sin[p(\alpha-\gamma)] + \mu_2\sin[p(\alpha-\beta)]\}}{D_{III}(p)} \tag{46}$$

where

$$D_{III}(p) = p(\mu_1+\mu_2)\sin(2p\alpha) \tag{47}$$

Eq. (47) is equal to Eq. (23), so the order of the stress singularity is the same as that in Problem I.

The displacement and stress fields are derived as

$$W_{III}^{(j)}(r,\theta) = \frac{2Fa}{(\mu_1+\mu_2)\pi} \times \sum_{n=1}^{\infty}\left\{\begin{array}{l} \dfrac{2}{2n-1}\left\{\cos\left[\dfrac{(2n-1)\pi}{2\alpha}\beta\right] - \cos\left[\dfrac{(2n-1)\pi}{2\alpha}\gamma\right]\right\}\cos\left[\dfrac{(2n-1)\pi}{2\alpha}\theta\right]\left(\dfrac{r}{a}\right)^{(2n-1)\pi/2\alpha} \\ +\dfrac{1}{n}\left[R^{j-1}\sin\left(\dfrac{n\pi\gamma}{\alpha}\right) + R^{j-2}\sin\left(\dfrac{n\pi\beta}{\alpha}\right)\right]\sin\left(\dfrac{n\pi\theta}{\alpha}\right)\left(\dfrac{r}{a}\right)^{n\pi/\alpha} \end{array}\right\} \tag{48}$$

$$\tau_{rz,III}^{(j)}(r,\theta) = \frac{2F}{(R+1)\alpha} \times \sum_{n=1}^{\infty}\left\{\begin{array}{l} R^{2-j}\left\{\cos\left[\dfrac{(2n-1)\pi}{2\alpha}\beta\right] - \cos\left[\dfrac{(2n-1)\pi}{2\alpha}\gamma\right]\right\}\cos\left[\dfrac{(2n-1)\pi}{2\alpha}\theta\right]\left(\dfrac{r}{a}\right)^{((2n-1)\pi/2\alpha)-1} \\ +\left[R\sin\left(\dfrac{n\pi\gamma}{\alpha}\right) + \sin\left(\dfrac{n\pi\beta}{\alpha}\right)\right]\sin\left(\dfrac{n\pi\theta}{\alpha}\right)\left(\dfrac{r}{a}\right)^{(n\pi/\alpha)-1} \end{array}\right\} \tag{49}$$

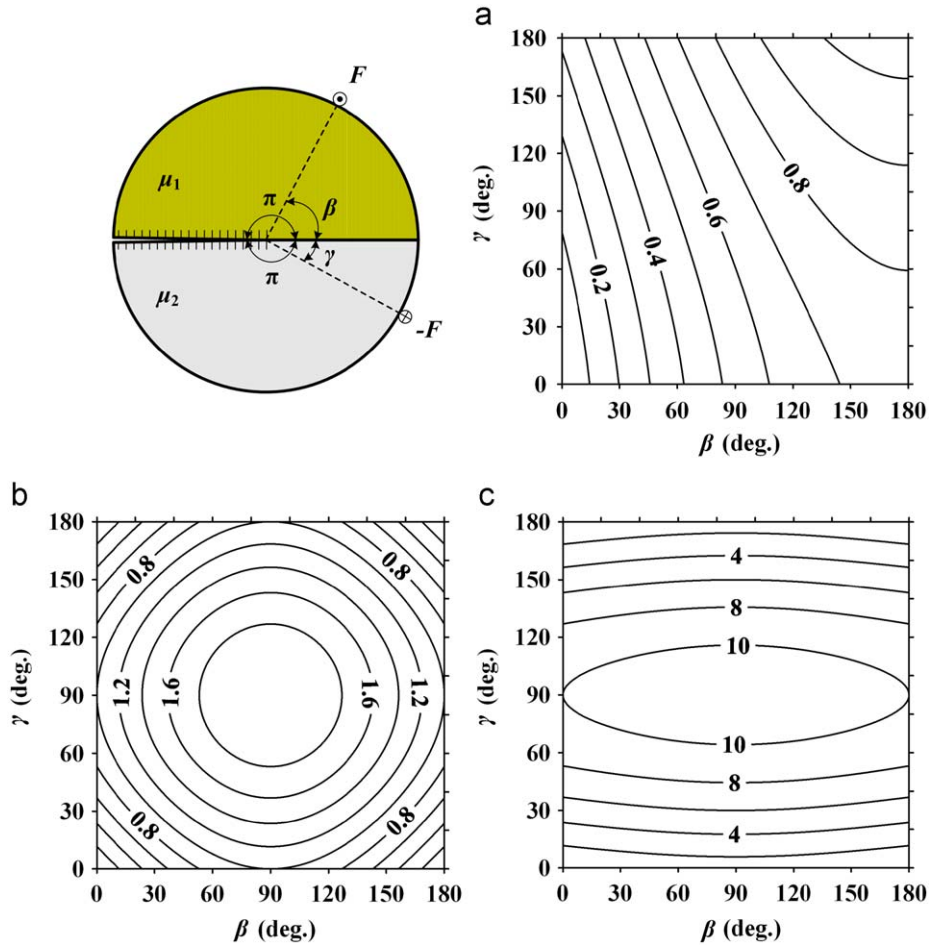

Fig. 5. $T_{\mathrm{III}}^{(\mathrm{III})}$ distributions for γ versus β in Problem III. (a) $R=0.1$, (b) $R=1$, (c) $R=10$.

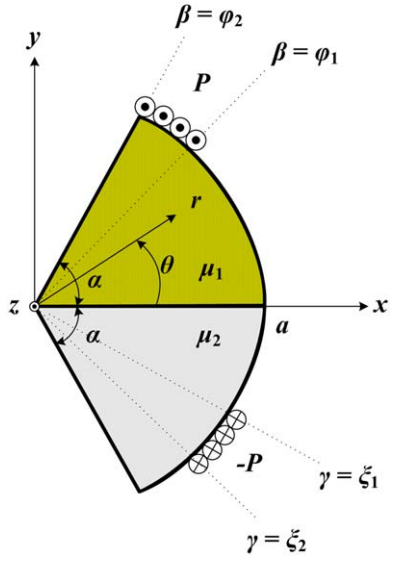

Fig. 6. Studied case with a pair of shear pressures.

$$\tau^{(j)}_{\theta z,\mathrm{III}}(r,\theta)=\frac{-2F}{(R+1)\alpha}\times\sum_{n=1}^{\infty}\left\{\begin{array}{l}R^{2-j}\left\{\cos\left[\dfrac{(2n-1)\pi}{2\alpha}\beta\right]-\cos\left[\dfrac{(2n-1)\pi}{2\alpha}\gamma\right]\right\}\sin\left[\dfrac{(2n-1)\pi}{2\alpha}\theta\right]\left(\dfrac{r}{a}\right)^{((2n-1)\pi/2\alpha)-1}\\-\left[R\sin\left(\dfrac{n\pi\gamma}{\alpha}\right)+\sin\left(\dfrac{n\pi\beta}{\alpha}\right)\right]\cos\left(\dfrac{n\pi\theta}{\alpha}\right)\left(\dfrac{r}{a}\right)^{(n\pi/\alpha)-1}\end{array}\right\}\tag{50}$$

If $\beta=\gamma$ and $\theta=0$, $\tau^{(j)}_{rz,\mathrm{III}}$ and $W^{(j)}_{\mathrm{III}}$ are reduced to zero, which is similar to the results obtained in Problem I. In this case, the problem can be regarded as two single material problems for which both radial edges are fixed.

When $\alpha=\pi$, a uniform $\tau^{(j)}_{\theta z,\mathrm{III}}$ is found at $\theta=0$ as

$$\lim_{r\to 0}\tau^{(j)}_{\theta z,III}(r,0)=\frac{2F}{(R+1)\pi}[R\sin(\gamma)+\sin(\beta)]\tag{51}$$

The following normalized expression is used for this uniform stress:

$$T^{(\mathrm{III})}_{\mathrm{III}}=\frac{(R+1)\pi}{2F}\lim_{r\to 0}\tau^{(j)}_{\theta z,\mathrm{III}}(r,0)\tag{52}$$

The $T^{(\mathrm{III})}_{\mathrm{III}}$ distributions for γ versus β with $R=0.1$, 1, and 10 are plotted in Fig. 5. Symmetric behavior of $T^{(\mathrm{III})}_{\mathrm{III}}$ can be observed for $0\le\beta\le 90^\circ$ and $90^\circ\le\beta\le 180^\circ$ with $R=0.1$; and for $0\le\gamma\le 90^\circ$ and $90^\circ\le\gamma\le 180^\circ$ with $R=10$. The loading angle of the softer material dominates the magnitude of $T^{(\mathrm{III})}_{\mathrm{III}}$.

Using the definition in Eq. (30), the SIF for this problem is

$$K^{(\mathrm{III})}_{\mathrm{III}}=0\tag{53}$$

$K^{(\mathrm{III})}_{\mathrm{III}}=0$ because the traditional definition of SIF, Eq. (30), is according to the radial direction parallel to crack surfaces. Nonetheless, it should be noted that a singular $\tau^{(j)}_{\theta z,\mathrm{III}}$ occurs in directions other than $\theta=0$.

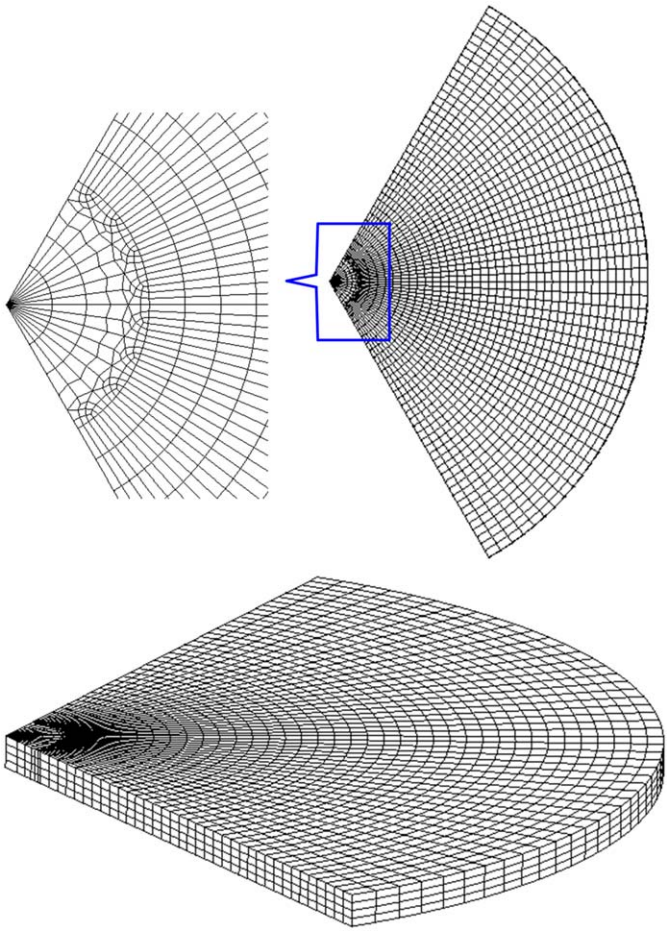

Fig. 7. Finite element meshes used for the case shown in Fig. 6.

3. A case study

In this section, a case with a pair of anti-plane shear pressures, P, shown in Fig. 6, is studied. The solutions for this case can be obtained by integrating the fundamental solutions (derived in Section 2) with respect to the loading range as

$$W^{(j)}_{\text{arc},\Lambda}(r,\theta) = \int_{\gamma=\xi_1}^{\gamma=\xi_2}\int_{\beta=\varphi_1}^{\beta=\varphi_2} W^{(j)}_{\Lambda}(r,\theta)d\beta\, d\gamma \tag{54a}$$

$$\tau^{(j)}_{\text{arc }rz,\Lambda}(r,\theta) = \int_{\gamma=\xi_1}^{\gamma=\xi_2}\int_{\beta=\varphi_1}^{\beta=\varphi_2} \tau^{(j)}_{rz,\Lambda}(r,\theta)d\beta\, d\gamma \tag{54b}$$

$$\tau^{(j)}_{\text{arc }\theta z,\Lambda}(r,\theta) = \int_{\gamma=\xi_1}^{\gamma=\xi_2}\int_{\beta=\varphi_1}^{\beta=\varphi_2} \tau^{(j)}_{\theta z,\Lambda}(r,\theta)d\beta\, d\gamma \tag{54c}$$

where $\xi_{2-}\xi_1 = \varphi_2-\varphi_1$, and Λ = I, II, and III for Problems I, II, and III, respectively.

The explicit results are given in Appendix. Finite element results are used to compare the derived solutions. The FE program ANSYS was employed to compute displacement and stress solutions of a special case. The following geometric parameters were assumed: $a = 1$, $\alpha = 60^\circ$, $\varphi_1 = 45^\circ$, $\varphi_2 = 60^\circ$, $\xi_1 = 30^\circ$, and $\xi_2 = 45^\circ$; material constants: $\mu_1 = 4e9$ and $\mu_2 = 8e9$; and arc line loads: $P = 1e6$. A 3-D model with 8616 twenty-node isoparametric brick elements was used. Only one degree of freedom in the z-direction (the in-plane degrees of freedom were set to zero) was considered for modeling. The FE mesh is shown in Fig. 7. Surface loads were applied parallel to the z-direction on the area of the arc plane from $\theta = \varphi_1$ to $\theta = \varphi_2$ and from $\theta = -\xi_1$ to $\theta = -\xi_2$. Since the in-plane degrees of freedom were fixed, a uniform outcome in the z-direction was expected (each depth has the same outcome). To compare the results in a more

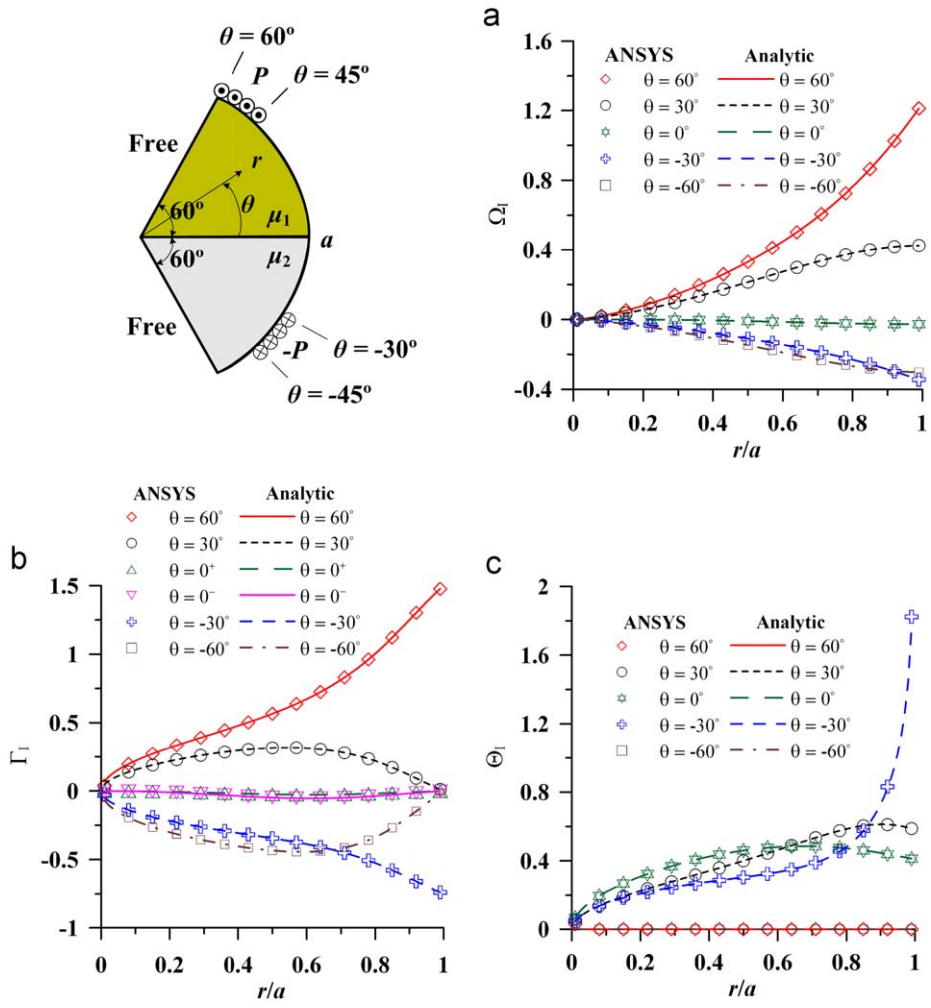

Fig. 8. Normalized solutions of the studied case compared with FE results for Problem I.

general form, we defined normalized expressions for the displacement and stresses as

$$\Omega_{\Lambda}^{(j)} = \frac{(\mu_1+\mu_2)}{Pa\alpha} W_{\mathrm{arc},\Lambda}^{(j)}(r,\theta) \tag{55a}$$

$$\Gamma_{\Lambda}^{(j)} = \frac{(R+1)}{P} \tau_{\mathrm{arc}\ rz,\Lambda}^{(j)}(r,\theta) \tag{55b}$$

$$\Theta_{\Lambda}^{(j)} = \frac{(R+1)}{P} \tau_{\mathrm{arc}\ \theta z,\Lambda}^{(j)}(r,\theta) \tag{55c}$$

It should be noted that the multiplier for the normalization is the constant obtained after integration in Eq. (54).

The FE results for Problems I, II, and III are compared with the analytical solutions (expanding Eq. (55) to 10,000 terms) in Figs. 8–10. Good agreement is achieved. Except for some critical locations for which FE fails to predict the correct stress fields, the discrepancy is well below 1%. These results verify that the fundamental solution derived in this study is appropriate and reliable.

4. Conclusions

Problems of composite finite wedges under anti-plane shear applied on a circular arc were solved using the finite Mellin transform in conjunction with the Laplace transform. The full-field solutions of displacements and stresses for various boundary edges, namely, free–free, free–fixed, and fixed–fixed, were derived explicitly. The SIF distributions of three considered problems for composite circular shafts with an interfacial crack are presented and discussed. For loads applied at equal angles, free–free and fixed–fixed edge problems can be degenerated into single material problems. Uniform stresses were found along the interface in free–free and fixed–fixed edge problems. A case with general loads was calculated and the results compared well with those obtained from FE analyses. The derived fundamental solutions can be used for further investigations.

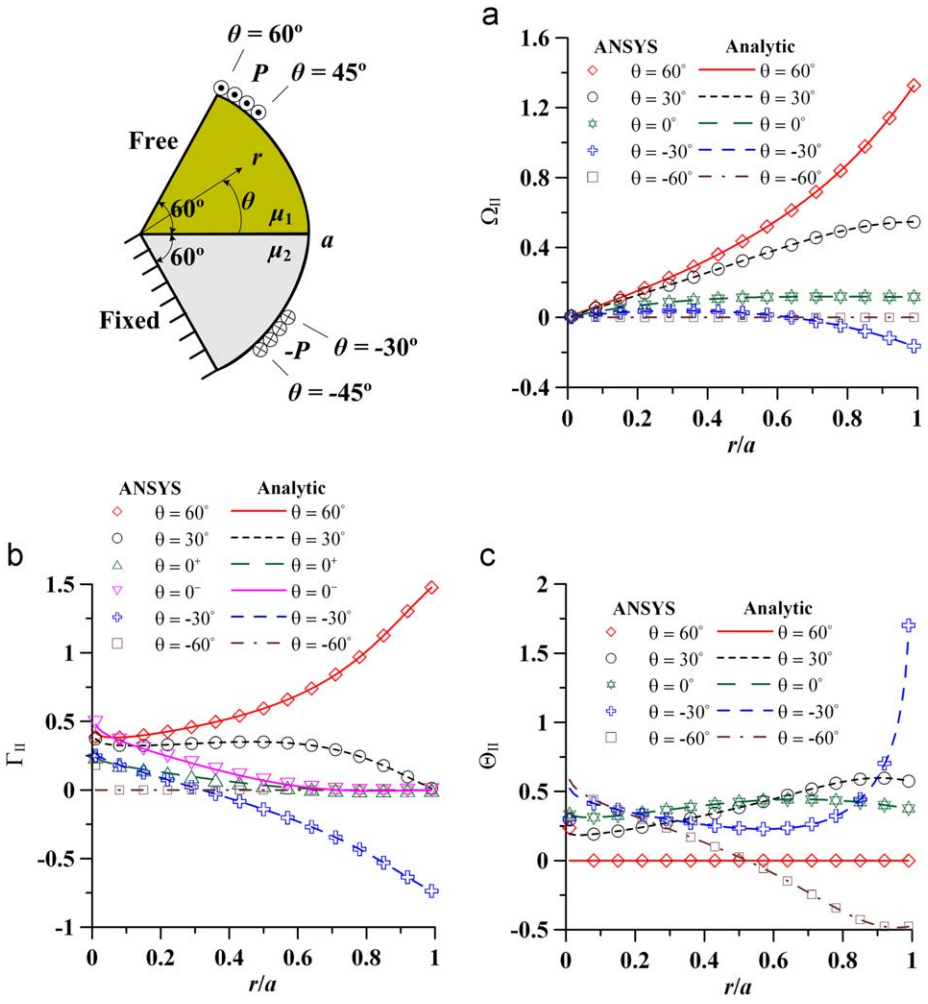

Fig. 9. Normalized solutions of the studied case compared with FE results for Problem II.

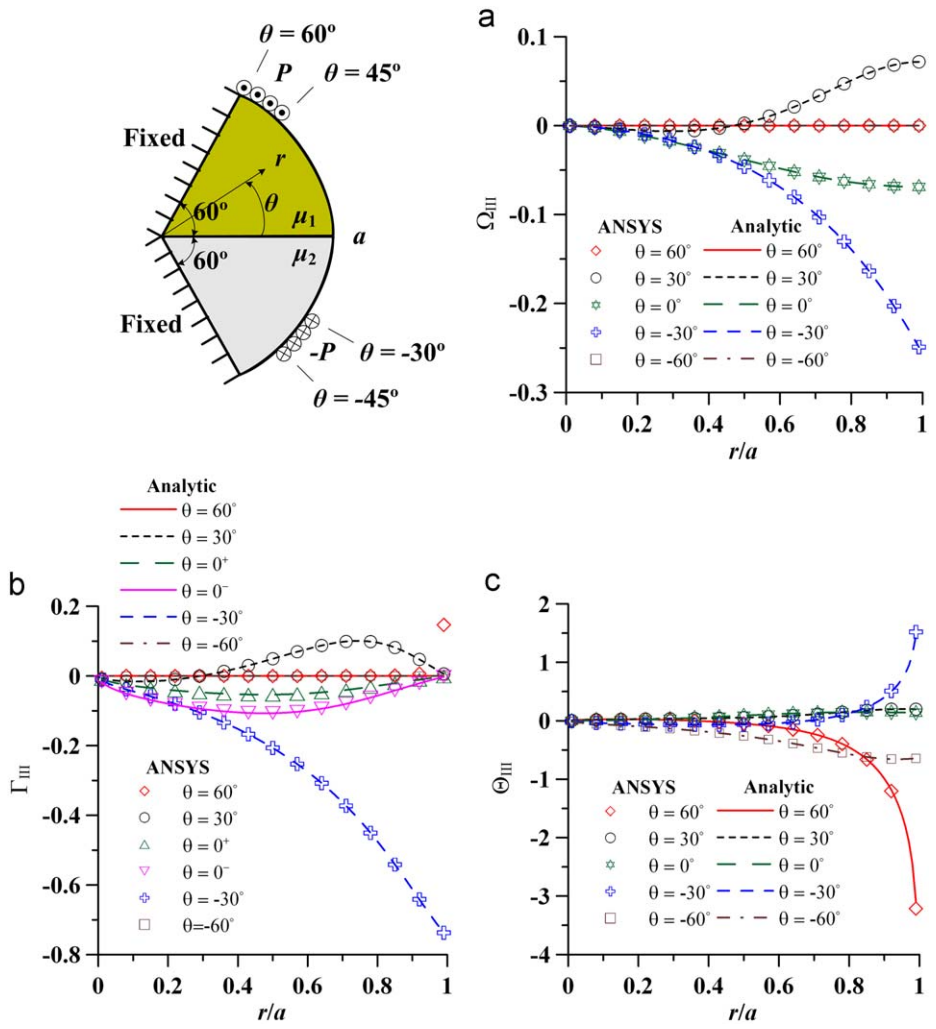

Fig. 10. Normalized solutions of the studied case compared with FE results for Problem III.

Appendix A. Explicit solutions for the studied case

For Problem I (free–free edge):

$$W^{(j)}_{\mathrm{arc,I}}(r,\theta)=\frac{Pa\alpha}{(\mu_1+\mu_2)}\sum_{n=1}^{\infty}\sum_{\ell=1}^{2}\frac{2(-1)^{\ell+1}}{\pi^2}\left\{\begin{array}{l}\left(\dfrac{2}{2n-1}\right)^2\left\{\begin{array}{l}R^{j-1}\cos\left[\dfrac{(2n-1)\pi}{2\alpha}\xi_\ell\right]\\ +R^{j-2}\cos\left[\dfrac{(2n-1)\pi}{2\alpha}\varphi_\ell\right]\end{array}\right\}\sin\left[\dfrac{(2n-1)\pi}{2\alpha}\theta\right]\left(\dfrac{r}{a}\right)^{(2n-1)\pi/2\alpha}\\ +\left(\dfrac{1}{n}\right)^2\left[\sin\left(\dfrac{n\pi\xi_\ell}{\alpha}\right)-\sin\left(\dfrac{n\pi\varphi_\ell}{\alpha}\right)\right]\cos\left(\dfrac{n\pi\theta}{\alpha}\right)\left(\dfrac{r}{a}\right)^{n\pi/\alpha}\end{array}\right\} \tag{A.1}$$

$$\tau^{(j)}_{\mathrm{arc}\ rz,\mathrm{I}}(r,\theta)=\frac{P}{(R+1)}\sum_{n=1}^{\infty}\sum_{\ell=1}^{2}\frac{2(-1)^{\ell+1}}{\pi}\left\{\begin{array}{l}\left(\dfrac{2}{2n-1}\right)\left\{\begin{array}{l}R\cos\left[\dfrac{(2n-1)\pi}{2\alpha}\xi_\ell\right]\\ +\cos\left[\dfrac{(2n-1)\pi}{2\alpha}\varphi_\ell\right]\end{array}\right\}\sin\left[\dfrac{(2n-1)\pi}{2\alpha}\theta\right]\left(\dfrac{r}{a}\right)^{((2n-1)\pi/2\alpha)-1}\\ +R^{2-j}\left(\dfrac{1}{n}\right)\left[\sin\left(\dfrac{n\pi\xi_\ell}{\alpha}\right)-\sin\left(\dfrac{n\pi\varphi_\ell}{\alpha}\right)\right]\cos\left(\dfrac{n\pi\theta}{\alpha}\right)\left(\dfrac{r}{a}\right)^{(n\pi/\alpha)-1}\end{array}\right\} \tag{A.2}$$

$$\tau^{(j)}_{\mathrm{arc}\ \theta z,\mathrm{I}}(r,\theta)=\frac{P}{(R+1)}\sum_{n=1}^{\infty}\sum_{\ell=1}^{2}\frac{2(-1)^{\ell+1}}{\pi}\left\{\begin{array}{l}\left(\dfrac{2}{2n-1}\right)\left\{\begin{array}{l}R\cos\left[\dfrac{(2n-1)\pi}{2\alpha}\xi_\ell\right]\\ +\cos\left[\dfrac{(2n-1)\pi}{2\alpha}\varphi_\ell\right]\end{array}\right\}\cos\left[\dfrac{(2n-1)\pi}{2\alpha}\theta\right]\left(\dfrac{r}{a}\right)^{((2n-1)\pi/2\alpha)-1}\\ -R^{2-j}\left(\dfrac{1}{n}\right)\left[\sin\left(\dfrac{n\pi\xi_\ell}{\alpha}\right)-\sin\left(\dfrac{n\pi\varphi_\ell}{\alpha}\right)\right]\sin\left(\dfrac{n\pi\theta}{\alpha}\right)\left(\dfrac{r}{a}\right)^{(n\pi/\alpha)-1}\end{array}\right\} \tag{A.3}$$

For Problem II (free–fixed edge):

$$W^{(j)}_{\text{arc,II}}(r,\theta)=\frac{Pa}{(\mu_1+\mu_2)}\sum_{m=1}^{\infty}\sum_{\ell=1}^{2}\frac{2(-1)^{\ell+1}}{p_m^2\alpha\,\sin(2p_m\alpha)}\left\{\begin{array}{l}\left\{\begin{array}{l}\sin(p_m\alpha)\sin[p_m(\alpha-\varphi_\ell)]\\+\cos(p_m\alpha)\cos[p_m(\alpha-\xi_\ell)]\end{array}\right\}\cos(p_m\theta)\\+\left\{\begin{array}{l}R^{j-1}\sin(p_m\alpha)\cos[p_m(\alpha-\xi_\ell)]\\+R^{j-2}\cos(p_m\alpha)\sin[p_m(\alpha-\varphi_\ell)]\end{array}\right\}\sin(p_m\theta)\end{array}\right\}\left(\frac{r}{a}\right)^{p_m} \tag{A.4}$$

$$\tau^{(j)}_{\text{arc }rz,\text{II}}(r,\theta)=\frac{Pa}{(R+1)}\sum_{m=1}^{\infty}\sum_{\ell=1}^{2}\frac{2(-1)^{\ell+1}}{p_m\alpha\,\sin(2p_m\alpha)}\left\{\begin{array}{l}\left\{\begin{array}{l}R\,\sin(p_m\alpha)\cos[p_m(\alpha-\xi_\ell)]\\+\cos(p_m\alpha)\sin[p_m(\alpha-\varphi_\ell)]\end{array}\right\}\sin(p_m\theta)\\+R^{2-j}\left\{\begin{array}{l}\sin(p_m\alpha)\sin[p_m(\alpha-\varphi_\ell)]\\+\cos(p_m\alpha)\cos[p_m(\alpha-\xi_\ell)]\end{array}\right\}\cos(p_m\theta)\end{array}\right\}\left(\frac{r}{a}\right)^{p_m-1} \tag{A.5}$$

$$\tau^{(j)}_{\text{arc }\theta z,\text{II}}(r,\theta)=\frac{Pa}{(R+1)}\sum_{m=1}^{\infty}\sum_{\ell=1}^{2}\frac{2(-1)^{\ell+1}}{p_m\alpha\,\sin(2p_m\alpha)}\left\{\begin{array}{l}\left\{\begin{array}{l}R\sin(p_m\alpha)\cos[p_m(\alpha-\xi_\ell)]\\+\cos(p_m\alpha)\sin[p_m(\alpha-\varphi_\ell)]\end{array}\right\}\cos(p_m\theta)\\-R^{2-j}\left\{\begin{array}{l}\sin(p_m\alpha)\sin[p_m(\alpha-\varphi_\ell)]\\+\cos(p_m\alpha)\cos[p_m(\alpha-\xi_\ell)]\end{array}\right\}\sin(p_m\theta)\end{array}\right\}\left(\frac{r}{a}\right)^{p_m-1} \tag{A.6}$$

where

$$p_m=\begin{cases}p_{m=2n-1}=\dfrac{1}{\alpha}\left[\tan^{-1}\left(\sqrt{\dfrac{1}{R}}\right)+(n-1)\pi\right],\\ p_{m=2n}=\dfrac{1}{\alpha}\left[n\pi-\tan^{-1}\left(\sqrt{\dfrac{1}{R}}\right)\right],\end{cases}\qquad n\in N \tag{A.7}$$

For Problem III (fixed–fixed edge):

$$W^{(j)}_{\text{arc,III}}(r,\theta)=\frac{Pa\alpha}{(\mu_1+\mu_2)}\sum_{n=1}^{\infty}\sum_{\ell=1}^{2}\frac{2(-1)^{\ell+1}}{\pi^2}\left\{\begin{array}{l}\left(\dfrac{2}{2n-1}\right)^2\left\{\begin{array}{l}\sin\left[\dfrac{(2n-1)\pi}{2\alpha}\xi_\ell\right]\\-\sin\left[\dfrac{(2n-1)\pi}{2\alpha}\varphi_\ell\right]\end{array}\right\}\cos\left[\dfrac{(2n-1)\pi}{2\alpha}\theta\right]\left(\dfrac{r}{a}\right)^{(2n-1)\pi/2\alpha}\\+\left(\dfrac{1}{n}\right)^2\left[R^{j-1}\cos\left(\dfrac{n\pi\xi_\ell}{\alpha}\right)+R^{j-2}\cos\left(\dfrac{n\pi\varphi_\ell}{\alpha}\right)\right]\sin\left(\dfrac{n\pi\theta}{\alpha}\right)\left(\dfrac{r}{a}\right)^{n\pi/\alpha}\end{array}\right\} \tag{A.8}$$

$$\tau^{(j)}_{\text{arc }rz,\text{III}}(r,\theta)=\frac{P}{(R+1)}\sum_{n=1}^{\infty}\sum_{\ell=1}^{2}\frac{2(-1)^{\ell+1}}{\pi}\left\{\begin{array}{l}R^{2-j}\left(\dfrac{2}{2n-1}\right)\left\{\begin{array}{l}\sin\left[\dfrac{(2n-1)\pi}{2\alpha}\xi_\ell\right]\\-\sin\left[\dfrac{(2n-1)\pi}{2\alpha}\varphi_\ell\right]\end{array}\right\}\cos\left[\dfrac{(2n-1)\pi}{2\alpha}\theta\right]\left(\dfrac{r}{a}\right)^{((2n-1)\pi/2\alpha)-1}\\+\left(\dfrac{1}{n}\right)\left[R\cos\left(\dfrac{n\pi\xi_\ell}{\alpha}\right)+\cos\left(\dfrac{n\pi\varphi_\ell}{\alpha}\right)\right]\sin\left(\dfrac{n\pi\theta}{\alpha}\right)\left(\dfrac{r}{a}\right)^{(n\pi/\alpha)-1}\end{array}\right\} \tag{A.9}$$

$$\tau^{(j)}_{\text{arc }\theta z,\text{III}}(r,\theta)=\frac{P}{(R+1)}\sum_{n=1}^{\infty}\sum_{\ell=1}^{2}\frac{2(-1)^{\ell+1}}{\pi}\left\{\begin{array}{l}-R^{2-j}\left(\dfrac{2}{2n-1}\right)\left\{\begin{array}{l}\sin\left[\dfrac{(2n-1)\pi}{2\alpha}\xi_\ell\right]\\-\sin\left[\dfrac{(2n-1)\pi}{2\alpha}\varphi_\ell\right]\end{array}\right\}\sin\left[\dfrac{(2n-1)\pi}{2\alpha}\theta\right]\left(\dfrac{r}{a}\right)^{((2n-1)\pi/2\alpha)-1}\\+\left(\dfrac{1}{n}\right)\left[R\cos\left(\dfrac{n\pi\xi_\ell}{\alpha}\right)+\cos\left(\dfrac{n\pi\varphi_\ell}{\alpha}\right)\right]\cos\left(\dfrac{n\pi\theta}{\alpha}\right)\left(\dfrac{r}{a}\right)^{(n\pi/\alpha)-1}\end{array}\right\} \tag{A.10}$$

References

[1] Tranter CJ. The use of the Mellin transform in finding the stress distribution in an infinite wedge. Q J Mech Appl Math 1948;1:125–30.
[2] Bogy DB. Two edge-bonded elastic wedges of different materials and wedge angles under surface tractions. J Appl Mech–Trans ASME 1971;38:377–86.
[3] Bogy DB. The plane solution for anisotropic elastic wedges under normal and shear loading. J Appl Mech–Trans ASME 1972;39:1103–9.
[4] Hein VL, Erdogan F. Stress singularities in a two-material wedge. Int J Fract Mech 1971;7:317–30.
[5] Ma CC, Wu HW. Analysis of inplane composite wedges under traction-displacement or displacement-displacement boundary conditions. Acta Mech 1990;85:149–67.
[6] Dempsey JP, Sinclair GB. On the stress singularities in the plane elasticity of the composite wedge. J Elasticity 1979;9:373–91.
[7] Dempsey JP, Sinclair GB. On the singular behavior at the vertex of a bi-material wedge. J Elasticity 1981;11:317–27.
[8] Bogy DB, Wang KC. Stress singularities at interface corners in bonded dissimilar isotropic elastic materials. Int J Solids Struct 1971;7:993–1005.
[9] Delale F. Stress singularities in bonded anisotropic materials. Int J Solids Struct 1984;20:31–40.
[10] Ting TCT. Anisotropic elasticity theory and applications. New York: Oxford University Press; 1996.
[11] Erdoagn F, Gupta GD. Bonded wedges with an interface crack under anti-plane shear loading. Int J Fract 1975;11:583–93.
[12] Ma CC, Hour BL. Analysis of dissimilar anisotropic wedges subjected to antiplane shear deformation. Int J Solids Struct 1989;11:1295–309.
[13] Shahani AR, Adibnazari S. Analysis of perfectly bonded wedges and bonded wedges with an interfacial crack under antiplane shear loading. Int J Solids Struct 2000;37:2639–50.

[14] Chue CH, Liu TJC. Electro-elastic analysis of a bimaterial piezoelectric wedge with an interface crack under antiplane concentrated forces and inplane surface charges. Int J Solids Struct 2004;41:4179–96.
[15] Li XF, Fan TY. Semi-infinite anti-plane crack in a piezoelectric material. Int J Fract 2000;102:L55–60.
[16] Shahani AR. Some problems in the antiplane shear deformation of bi-material wedges. Int J Solids Struct 2005;42:3093–113.
[17] Bera B, Patra B. On the shear of an elastic wedge as a mixed boundary value problem. Acta Mech 1979;33:307–16.
[18] Kargarnovin MH, Shahani AR, Fariborz SJ. Analysis of an isotropic finite wedge under antiplane deformation. Int J Solids Struct 1997;34:113–28.
[19] Chue CH, Liu WJ. Antiplane electro-mechanical field of a piezoelectric finite wedge under shear loading and at fixed-grounded boundary conditions. Int J Solids Struct 2007;44:2540–52.
[20] Shahani AR. Mode III stress intensity factors for edge-crack circular shafts, bonded wedges, bonded half planes and DCB's. Int J Solids Struct 2003;40:6567–76.
[21] Lin RL, Ma CC. Theoretical full-field analysis of dissimilar isotropic composite annular wedges under anti-plane deformations. Int J Solids Struct 2004;41:6041–80.
[22] Noda NA, Takase Y, Hamashima T. Generalized stress intensity factors in the interaction within a rectangular array of rectangular inclusions. Arch Appl Mech 2003;73:311–22.
[23] Chen MC, Ping XC. Analysis of the interaction within a rectangular array of rectangular inclusions using a new hybrid finite element method. Eng Fract Mech 2009;76:580–93.
[24] Sneddon IN. The use of integral transforms. New York: McGraw-Hill; 1972.